

DeepEigen: Learning-based Modal Sound Synthesis with Acoustic Transfer Maps

Xutong Jin*
Peking University

jinxutong@pku.edu.cn

Sheng Li*
Peking University

lisheng@pku.edu.cn

Dinesh Manocha
University of Maryland

dmanocha@umd.edu

Guoping Wang
Peking University

wgp@pku.edu.cn

Abstract

We present a novel learning-based approach to compute the eigenmodes and acoustic transfer data for the sound synthesis of arbitrary solid objects. Our approach combines two network-based solutions to formulate a complete learning-based 3D modal sound model. This includes a 3D sparse convolution network as the eigendecomposition solver and an encoder-decoder network for the prediction of the Far-Field Acoustic Transfer maps (FFAT Maps). We use our approach to compute the vibration modes (eigenmodes) and FFAT maps for each mode (acoustic data) for arbitrary-shaped objects at interactive rates without any precomputed dataset for any new object. Our experimental results demonstrate the effectiveness and benefits of our approach. We compare its accuracy and efficiency with physically-based sound synthesis methods.

1. Introduction

3D modal sound models are widely used to synthesize rigid-body sounds in animation, games, and virtual environments. These methods usually precompute the eigenvectors and eigenfrequencies of a solid object or model [42, 31, 35, 3, 17, 26], which correspond to dense eigenmode matrix. This representation can be used to compute the sound model’s response to contact forces. These vibrations are linearly combined during sound synthesis. Since the human auditory system cannot directly hear an object’s vibration, acoustic transfer models are typically used to describe the sound pressure at a listener’s position. There is considerable research on improving the performance of these methods in terms of quality or runtime performance [45, 3, 47, 6, 38, 39].

Physically-based methods based on modal analysis for sound synthesis have been used in different applications. However, they have a few limitations. In particular, high-quality 3D modal sound models take a long time to pre-

compute eigenmode matrices (modal analysis) [42, 31] and acoustic transfer functions (usually boundary element method (BEM) analysis) [17, 43]. Many applications use different objects with varying shapes and they are unable to reuse this eigenmode data for other objects. Instead, we need to perform this pre-computation step for each object. The acoustic transfer computation using BEM analysis is substantially slower than modal analysis for sound synthesis [17]. Moreover, the uncompressed eigenmode data (tens to hundreds of megabytes) is much larger than acoustic transfer data and needs to be compressed [23]. As a result, prior methods are limited to rigid objects and can not handle deforming or breaking objects. Recently, learning methods have been proposed to accelerate the performance of sound simulation algorithms. These include network architectures for the sound synthesis of solid objects [19], musical instrument sound synthesis [14, 18], computing acoustic scattering functions [10, 41], etc.

Main Results: We present a novel learning-based approach for the sound synthesis of arbitrary solid objects, which also takes into account the acoustic transfer functions. We design a 3D sparse convolution-based U-Net, which is used as an approximation of traditional eigendecomposition solver. We also present an encoder-decoder network that is used to predict the Far-Field Acoustic Transfer maps (FFAT Maps) [5] from the surface vibration shape of an object. The eigenmode data predicted by our first network is used to predict the FFAT maps for each mode in the second network. The amplitude of the vibration mode is re-scaled by the FFAT map to synthesize the final audio. These two network-based solutions are combined to formulate a complete learning-based 3D modal sound model. Based on our approach, vibration modes (i.e., eigenmodes) and FFAT maps for each mode (acoustic data) for arbitrary-shaped objects can be interactively computed at runtime without any precomputed dataset for each new object. Therefore, the sound of objects corresponding to new shapes can also be synthesized at runtime. The runtime storage needed for our method is only in terms of network parameters. We also analyze the relationship between an eigenvalue decomposi-

*Equal Contribution

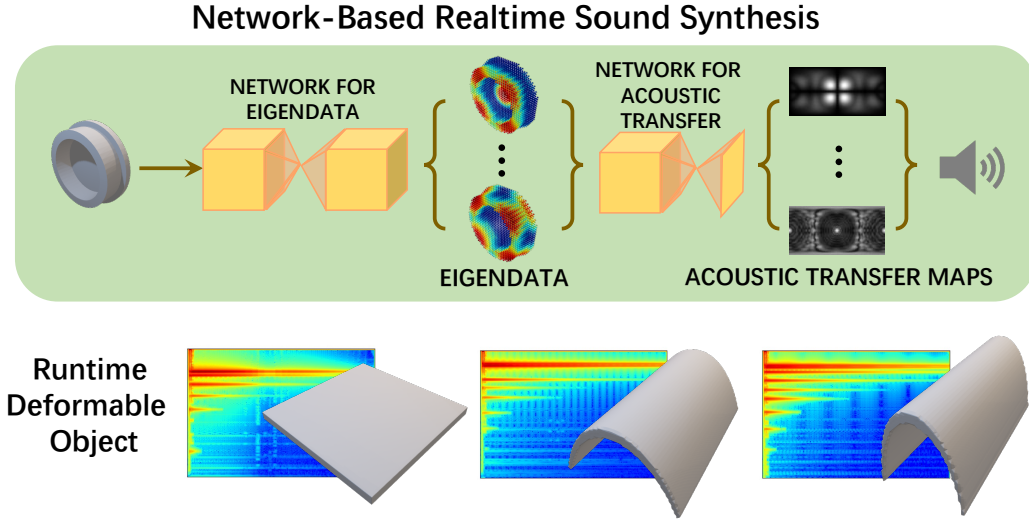


Figure 1. Our DeepEigen Architecture for Modal Sound Synthesis: Our learning-based approach, DeepEigen, uses deep networks to perform eigenmodes and acoustic transfer maps computations to synthesize the sound. We highlight our network at the top and its application to a deforming object at the bottom. Our approach can generate plausible sound effects in a few milliseconds on a GeForce GTX 1080 Ti GPU with no object-based precomputations.

tion iteration and the 3D sparse convolution network, which provides more insights and connections between our neural network architecture and modal analysis. Overall, our novel contributions include:

- We present a complete learning-based approach to compute the eigenmodes and acoustic transfer data. To the best of our knowledge, ours is the first learning-based method that can approximate the complete physically-based 3D modal sound synthesis pipeline that includes the acoustic transfer step.
- Our approach can handle objects corresponding to new shapes or typologies at runtime without any precomputations.
- Our formulation can generate plausible sound synthesis results in few milli-seconds on a GeForce GTX 1080 Ti GPU. We highlight results from a preliminary user study.
- We show theoretical connections between eigenvalue decomposition iteration and our 3D convolution network. This insight can be used to design better neural architectures for the sound synthesis and analyze their performance.

2. Related works

Modal Sound Synthesis Modal sound models are widely used in computer graphics and animations. Modal sound synthesis is a popular technique [8, 42, 31, 35] used to

synthesize sounds of a rigid body. These methods compute the characteristic vibration modes of a 3D object using eigendecomposition-based preprocessing. Many techniques are based on the use of 3D objects’ pre-computed eigenmatrix to perform runtime sound synthesis, e.g., using the parallel computing capabilities of the GPU to speedup the computation [45] or reduce the computational complexity by using approximations [3]. Other methods use more complex modal sound synthesis models to simulate sounds more accurately, including knocking, sliding, and friction on 3D objects [42], acceleration noise synthesis [6], accurate damping models [39] and contact models [47].

Precomputed Acoustic Transfer Precomputed acoustic transfer functions [17] are used to more accurately model the sound pressure at the listener’s position. Other techniques used a single-point multipole expansion with higher-order sources [47, 46, 23, 37] and inter-object transfer functions [29].

Precomputation Cost: Many methods focus on reducing the precomputation cost of modal sound synthesis and acoustic transfer functions. Li et al. [25] propose a method to enable interactive acoustic transfer evaluation so that there is no need to recalculate the acoustic transfer when changing an object’s material. KleinPAT [43] can accelerate acoustic transfer precomputation on the GPU by packing modes into several partitions. A deep neural network [19] is proposed to synthesize the sound of a rigid body of arbitrary shape being hit at runtime and predicts the amplitudes

and frequencies of sound directly. However the eigenmode data is lost and this approach cannot be applied to complex models.

Deep Learning Models: There is considerable work on exploring three-dimensional geometric features for learning, including perspective-based methods [40, 20], voxel-based methods [44, 28], and point cloud-based methods [34, 33]. Our formulation is based on the sparse voxel-based method [13, 12, 7] and we also derive new connections with modal analysis.

3. Background

In this section, we provide background on 3D modal sound synthesis. We begin with the linear deformation equation for a 3D linear elastic dynamics model:

$$\mathbf{M}\ddot{\mathbf{x}} + \mathbf{C}\dot{\mathbf{x}} + \mathbf{K}\mathbf{x} = \mathbf{f}, \quad (1)$$

where \mathbf{x} is nodal displacements and $\mathbf{M}, \mathbf{C} = \alpha\mathbf{M} + \beta\mathbf{K}, \mathbf{K}$ represent the mass, Rayleigh damping, and stiffness matrices, respectively. \mathbf{f} represents the external nodal forces, which excite the vibrations. Through generalized eigenvalue decomposition $\mathbf{K}\mathbf{U} = \mathbf{\Lambda}\mathbf{M}\mathbf{U}$, the system can be decoupled into the following form :

$$\ddot{\mathbf{q}} + (\alpha\mathbf{I} + \beta\mathbf{\Lambda})\dot{\mathbf{q}} + \mathbf{\Lambda}\mathbf{q} = \mathbf{U}^T\mathbf{f}, \quad (2)$$

where $\mathbf{\Lambda}$ is a diagonal matrix and \mathbf{q} satisfies $\mathbf{x} = \mathbf{U}\mathbf{q}$. The solution to the equation is a bank of damped sinusoidal waves. Each wave represents a mode. The i -th mode is:

$$q_i = a_i e^{-c_i t} \sin(\omega_i t + \theta_i), \quad (3)$$

where ω_i is the frequency of the mode (damped natural frequency), c_i is the damping coefficient, a_i is the excited amplitude, and θ_i is the initial phase with $i = 1, 2, \dots, m$. Note that the eigenmode data, \mathbf{U} , is used to project the contact forces \mathbf{f} into the modal subspace at runtime and needs to be stored after precomputation [23].

To synthesize high-quality modal sound, these methods need to take into account the acoustic transfer model. Without loss of generality, the sound at position x and time t can be expressed as

$$\sum_{i=1}^M |p_i(x)| q_i(t),$$

where $p_i(x)$ is the sound pressure generated by a unit amplitude vibration of mode i . After solving the acoustic transfer function of a small domain containing the vibration object, a practical representation is used for rapid evaluation during sound rendering, including Equivalent-Source Representations [17, 29], Multipole Source Representation [46], Far-Field Acoustic Transfer (FFAT) Maps

[5], etc. Precomputed acoustic transfer data is also stored for runtime sound rendering. We note that for each 3D object used in sound rendering, we need separate eigenmode data and acoustic transfer data. This increases the storage requirements.

4. learning based formulation

As mentioned in background, eigendecomposition and acoustic transfer are the two core concerns in sound synthesis. In this section, we introduce our formulations of the results of the classic solvers (i.e. Lanczo method for eigendecomposition and Boundary Element Method for acoustic transfer) and specify these formulations as the ground-truth of our learning-based solvers. Most importantly, we analyze the relationship between an classic eigendecomposition iteration algorithm and our neural network-based solver. This observation helps us design our network and can be used as an interpretability analysis tool of neural networks used for modal synthesis.

4.1. Modified Eigendecomposition Formulation

For sound synthesis, the range of eigenvalues is limited by the human audible perception range (usually 20HZ \sim 20000HZ). We divide the range of eigenvalue into m intervals, the upper and lower eigenvalues of the interval j is denoted as μ_j^+, μ_j^- which satisfies $\mu_{j-1}^+ = \mu_j^-$. Our modified eigendecomposition fomulation takes the linear combination of eigenvectors in each interval as the approximate eigenvector and the mean of eigenvalues in each interval as the approximate eigenvalue.

For a generalized eigendecomposition problem with mass matrix \mathbf{M} and stiff matrix \mathbf{K} , we denote the eigenvectors as \mathbf{v}_i and eigenvalues as λ_i ($1 \leq i \leq n$). Given a random initial vector \mathbf{b}_0 , it can be written as $\mathbf{b}_0 = \sum_{i=1}^n c_i \mathbf{v}_i$. Parameters c_i can be obtained using the projection $c_i = \mathbf{b}_0^T \mathbf{M} \mathbf{v}_i$. Our approximate eigenvector for interval j is defined as:

$$\hat{\mathbf{v}}_j = \sum_{(\mathbf{v}_i, \lambda_i) \in \Phi(j)} c_i \mathbf{v}_i \quad (4)$$

And the approximate eigenvalues for interval j is defined as :

$$\hat{\lambda}_j = \frac{1}{|\Phi(j)|} \sum_{(\mathbf{v}_i, \lambda_i) \in \Phi(j)} \lambda_i \quad (5)$$

Where $\Phi(j) = \{(\mathbf{v}, \lambda) \mid \mu_j^- \leq \lambda \leq \mu_j^+\}$ is the set of eigenvector-eigenvalue pairs in interval j .

In other words, we mix the modes with similar frequencies into one. The mixed frequency can be obtained from the mean eigenvalue. The mixed eigenvector is related with the initial vector and the mixed eigenvectors for different initial vectors are generally linearly independent, so unmixed eigenvectors can be recovered by extracting the basis of these mixed eigenvectors for better sound richness.

The approximate eigenvector and eigenvalue are used as the ground-truth for our learning-based eigen solver.

4.2. Simplified Acoustic Transfer Map Formulation

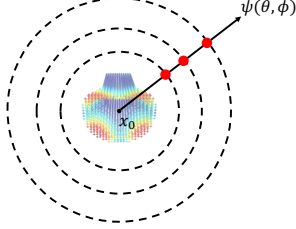


Figure 2. We highlight the FFAT map used for acoustic transfer function computation. The FFAT map values are estimated by the least square method for the 3 sample points shown.

We use the simplified Far-Field Acoustic Transfer (FFAT) map [5, 43] as the efficient representation of the acoustic transfer function. FFAT maps can perform fast transfer computations[16] and can be efficiently compressed [43]

This representation is based on the following characterization. Usually $p(\mathbf{x}) \in \mathbb{C}$ is used to represent the complex-valued sound pressure field, and is used to synthesize the final sound during sound rendering as: $\sum_{i=1}^M |p_i(\mathbf{x})| q_i(t)$, where $p_i(\mathbf{x})$ is the sound pressure generated by a unit amplitude vibration of mode i . We use a function ψ_i to approximate the directionality information of $|p_i(\mathbf{x})|$, and use $1/r$ to approximate the attenuation of the transfer amplitude as the radial distance increases:

$$\frac{\psi_i(\theta, \phi)}{r} \approx |p_i(\mathbf{r})|, \quad (6)$$

where r is evaluated with respect to the object’s bounding box center point, x_0 . θ, ϕ are the coordinates in the spherical coordinate system. Shoot a ray from x_0 at an angle (θ, ϕ) . The ray will intersect with N_s spheres with different radii. The value of $\psi_i(\theta, \phi)$ can be determined by the least square method based on the values of these intersection points. This is shown in Figure 2. We follow the settings in KleinPAT [43] and set $N_s = 3$ and the radius of these three spheres are computed as $R_i = (1.25a)^i, i = 1, 2, 3$, where a represents the longest side of the bounding box. In our current formulation, we ignore the radiation efficiency and standardize the FFAT map to a unit variance. The function ψ_i are used as the ground-truth for our learning-based acoustic solver

4.3. Connection between Network and Eigenmode Solver

We highlight intrinsic connections between the classic eigenmode solvers [1, 22, 21] and deep neural networks.

Later we use these connections to design our network architecture described in Section 5.

Assembled Matrix and 3D Sparse Convolution Assuming that we are working with a finite element model with N hexahedrons and M vertices, a assembled matrix (e.g. mass matrix or stiffness matrix) $\mathbf{A} \in \mathbb{R}^{3M \times 3M}$ is built by assembling the element matrix $\mathbf{A}_e \in \mathbb{R}^{24 \times 24}$ for all hexahedrons. $\mathbf{x} \in \mathbb{R}^{3M}$ is a vector of vertex displacement.

We denote a modified representation of vector \mathbf{x} as $\mathbf{x}' \in \mathbb{R}^{24N}$, which represent 8 vertex displacements of all hexahedrons. \mathbf{x}' is a equivalent expression of \mathbf{x} with some redundancy. So matrix-vector multiplication can be equivalently expressed as:

$$(\mathbf{A}\mathbf{x})'_{\mathbf{u}} = \sum_{\mathbf{i} \in \mathcal{N}(\mathbf{u})} \mathbf{F}(\mathbf{A}_e, \mathbf{i}) \mathbf{x}'_{\mathbf{i}+\mathbf{u}}, \quad (7)$$

Where $\mathbf{u} \in \mathbb{R}^3$ is the 3D coordinate of a hexahedron, $\mathcal{N}(\mathbf{u})$ is the set of offsets of all neighboring hexahedrons, and $\mathbf{F} \in \mathbb{R}^{24 \times 24}$ is a matrix related to \mathbf{A}_e (the element matrix) and \mathbf{i} (offset to neighbors).

The matrix \mathbf{F} can be represented by a kernel with weight $\mathbf{W} \in \mathbb{R}^{3^3 \times 24 \times 24}$ and the above equation is actually a 3D sparse convolution [7, 13, 12]. Note that weight W is only related to element matrix \mathbf{A}_e , so matrix multiplication with the same element matrix is equivalent to the same 3D sparse convolution for any model(i.e. with different shape).

Inverse Assembled Matrix and Sparse U-Net Multi-grid [4] is a fast algorithm for solving inverse matrix-vector multiplication using a hierarchy of discretizations: correction of the solution from a fine model to a coarse model then from the coarse model to the fine model. Each correction corresponds to a matrix-vector multiplication and equivalent to a corresponding 3D sparse convolution mentioned above. The whole process is equivalent to a corresponding 3D sparse U-Net [36]. Inverse matrix vector multiplication can also be solved by non-multiscale iterative method (e.g. Jacobi Method) and equivalent to a series of corresponding 3D sparse convolution.

Modified Formulation and Sparse Neural Network Combine the connections mentioned above, we know that a sparse neural network has the ability to approximate a polynomial of assembled matrix or related inverse matrix. Now we use a example to describe how such a polynomial of matrix transform a random vector into a eigenvalue related result.

For Equation 1, eigenvector \mathbf{v}_i and eigenvalue λ_i satisfies:

$$\mathbf{K}\mathbf{v}_i = \lambda_i \mathbf{M}\mathbf{v}_i \quad (8)$$

For a fixed value μ , we have:

$$(\mathbf{K} - \mu\mathbf{M})\mathbf{v}_i = (\lambda_i - \mu)\mathbf{M}\mathbf{v}_i \quad (9)$$

which derives this equation:

$$(\mathbf{K} - \mu\mathbf{M})^{-1}\mathbf{M}\mathbf{v}_i = \frac{1}{\lambda_i - \mu}\mathbf{v}_i \quad (10)$$

If we apply the matrix $(\mathbf{K} - \mu\mathbf{M})^{-1}\mathbf{M}$ to the random vector $\mathbf{b}_0 = \sum_{i=1}^n c_i \mathbf{v}_i$, we get a eigenvalue related result:

$$\begin{aligned} (\mathbf{K} - \mu\mathbf{M})^{-1}\mathbf{M}\mathbf{b}_0 &= \sum_{i=1}^n c_i (\mathbf{K} - \mu\mathbf{M})^{-1}\mathbf{M}\mathbf{v}_i \\ &= \sum_{i=1}^n \frac{c_i}{\lambda_i - \mu} \mathbf{v}_i \end{aligned} \quad (11)$$

where the eigenvectors with eigenvalue far from μ are weaken and the eigenvectors with eigenvalue close to μ are strengthen.

Similar matrix polynomial can be approximated by a sparse neural network and can transform a random vector to linear combination of eigenvectors with eigenvalue close to μ . This is why we designed such a modified formulation in ?? . And we emphasize that the property in Equation 11 is independent on the shape of 3D model, so our network-based eigen solver can handle 3D models of arbitrary shapes.

5. MODULAR ARCHITECTURE

In this section, we present our designed modular architectures of network-based eigen solver EigenNet and acoustic transfer solver AcousticNet. Here, we only consider computing the eigenmode and acoustic transfer data of objects with fixed materials and fixed scales in the network architecture. A post-processing step, similar to DeepModal [19], can be used to integrate different material parameters and sizes. In contrast to the prior deep learning-based method, DeepModal [19], which directly predicts the sound of object without considering the acoustic transfer, our two independent modular components predict eigen-data and acoustic transfer map respectively and can be used alone to replace the corresponding part in the traditional method.

5.1. Eigendecomposition Module: EigenNet

Our eigendecomposition module, EigenNet, consists of two branches: Shape branch and Frequency branch. As mentioned in subsection 4.3, we used 3D sparse convolution as basic block in our modules. Rectified linear unit (ReLU) and batch normalization are used after each convolution. For more details about 3D sparse convolution, the reader can refer to [7, 13, 12].

5.1.1 Shape Branch

The core of the Shape branch in EigenNet is a 3D sparse U-Net[36]. As the pre-processing, we voxelized 3D objects to voxel models and then project initial vectors and approximate eigenvectors mentioned in subsection 4.1 to sparse tensors. For each voxel, the projection is actually interpolating from the vertices to the center. As eigenvector consists the feature in x, y, z direction for each vertex, one eigenvector is projected to three sparse tensors.

After projection, we denote the initial sparse tensor as \mathbf{F}_{rand} and the approximate eigenvector sparse tensor as $\mathbf{F}_{\text{shape}}$. The 3D sparse U-Net is trained to predict $\mathbf{F}_{\text{shape}}$ from input \mathbf{F}_{rand} . We designed input \mathbf{F}_{rand} as single channel and output $\mathbf{F}_{\text{shape}}$ as multi channel, each three channel corresponds to the approximation eigenvector in one interval. See Figure 3

6. learning-based solver for Acoustic Transfer Functions

In this section, we present our learning-based acoustic transfer data solver. This transfer function between the input and output is simpler than eigenmode computation: the surface vibration of a mode affects the surrounding air and the sound pressure field is formed. We design a learning-based solver to take a mode surface shape as input and predict an FFAT Map image.

6.1. Acoustic Transfer Computation

In this section, we describe our learning-based solver for acoustic transfer computation. We use a coordinate matrix $\mathbf{C} \in \mathbb{Z}^{N \times 3}$ to represent the coordinates of surface voxels on an object, where N is the number of surface voxels. We use an associated feature matrix $\mathbf{F}_{\text{shape}} \in \mathbb{R}^{N \times 3}$ to represent the mode shape of the surface voxel, which is part of an eigenvector.

Vibration frequency is another important parameter that is used to compute the transfer functions. For simplicity, we currently only consider a limited number of frequencies: frequencies matching the central eigenvalues in interval mentioned in ?? . We use a one-hot vector \mathbf{h} to represent the frequency, where $h_j = 1$ means the frequency matching the center value of j th eigenvalue interval (the matching relationship is $f = \frac{\sqrt{\mu_j}}{2\pi}$).

$\mathbf{C}, \mathbf{F}_{\text{shape}}, \mathbf{h}$ together form the input of the learning-based solver. The output of the learning-based solver is an FFAT map $\psi \in \mathbb{R}^{+^{r \times 2r}}$, where $r \times 2r$ is the image resolution of the FFAT map. Overall, we denote the learning-based solver as \mathbf{g}_e , which is a neural network with weights θ_e and satisfies:

$$\mathbf{g}_e(\mathbf{C}, \mathbf{F}_{\text{shape}}, \mathbf{h}; \theta_e) = \psi. \quad (12)$$

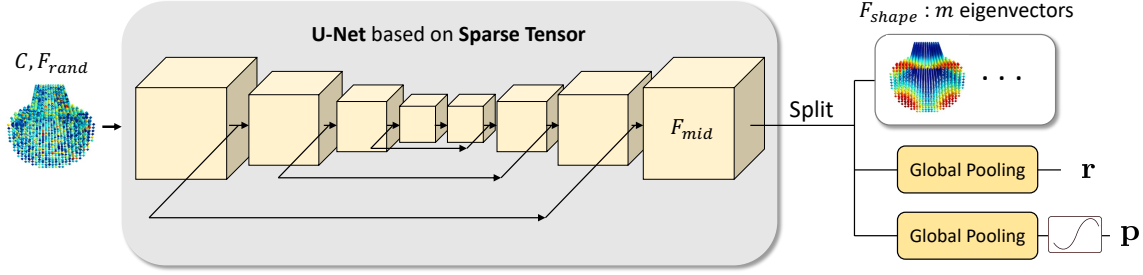


Figure 3. We highlight our network architecture used for learning-based eigenmode solver. A U-Net takes randomly-initialized vector F_{rand} with coordinates C as input and outputs F_{shape}, r, p . F_{shape}, r, p are separated from the feature maps F_{mid} . As r, p represent global features of the object, they are within the global average pooling layer.

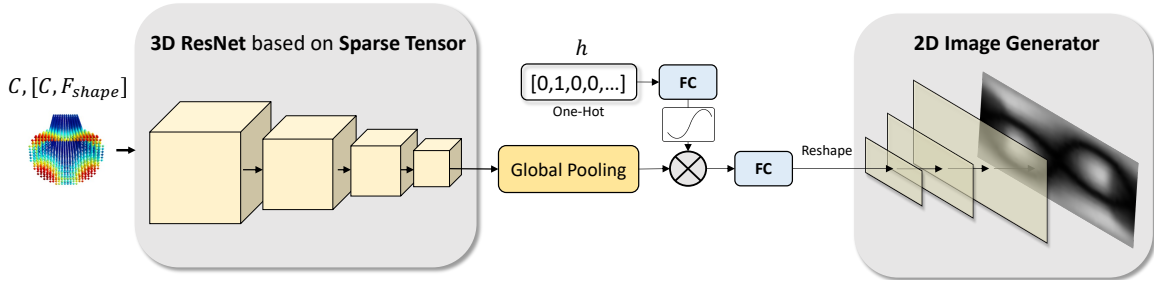


Figure 4. The network architecture of our learning-based solver for acoustic transfer data computation. The eigenvector (mode shape) matrix F_{shape} and coordinate matrix C are used as inputs into a 3D ResNet. The output feature is embedded with the one-hot vector h and sent into a 2D image generator to predict the FFAT map.

The loss function is defined as: $(\|\psi - \hat{\psi}\|_2)^2$, with a mean squared error (MSE) for the FFAT map. It should be noted that the input and output of the network are related to only one mode of the object, but all modes can be processed in parallel through a mini-batch.

6.2. Network Architecture

To bridge the 3D surface vibration shape of the object with an FFAT map, we use an encoder-decoder structure [36, 27, 30]. The encoder part is a sparse tensor-based 3D ResNet [15] and the decoder part is a 2D image generator [11]. Rectified linear unit (ReLU) and batch normalization are used after each convolution and transposed convolution (not including the last one). The overall architecture of our network is shown in Figure 4.

The 3D ResNet takes surface coordinate matrix C and surface mode shape matrix F_{shape} as inputs. As the coordinate information is used for solving the FFAT map, we normalize and concatenate the coordinate matrix C into the shape matrix F_{shape} . The 3D ResNet extracts the global latent features and passes them into the 2D image generator. To embed the frequency information into the global latent feature, we project the one-hot vector to a weight by a fully connected (FC) layer and a sigmoid activation function. The weight is used to multiply the global latent feature

and update it. The weight shows the importance of each latent feature at the current frequency. Finally, the updated global feature is projected and reshaped to the first layer in the 2D image generator.

7. Overall modal sound model

Based on our solvers for eigenmode computation and acoustic transfer data, we formulate a complete modal sound model. For a 3D object, we use our learning-based solver to compute the m eigenvectors for m eigenvalue intervals from one randomly initialized vector. Next, these eigenvectors are used as an input to the second learning-based solver to compute m corresponding FFAT maps in parallel.

To solve the eigenvectors more accurately, we use t random initial vectors and solve $t \times m$ approximation eigenvectors, with t eigenvectors per interval. These can be processed in parallel by constructing mini-batch data in our network. As mentioned in ??, t approximation eigenvectors in an interval are different linear combinations of the actual eigenvectors within this interval. Therefore, we apply principal component analysis (PCA) to these approximate eigenvectors to estimate several eigenvectors with improved accuracy. Then these eigenvectors are used to compute the

corresponding FFAT maps. As *Rayleigh quotients* and interval probabilities are computed t times, we use their average in the final result.

8. Implementation and Performance

8.1. Dataset

The 3D models we use for training are the Thingi10k [48] dataset. Thingi10k dataset contains about 10,000 3D models collected from an online 3D printing model-sharing database and represents a more concise summary of the real-world. We voxelized these 3D models with a resolution of $32 \times 32 \times 32$ as part of the preprocessing.

Next, we compute the dataset for the eigenmode matrices. For every object, we use a finite element model with a specific material, e.g., ceramic, and formulate Equation 1. Next, we perform generalized eigenvalue decomposition based on the Lanczos Method [24]. To reduce the overall preprocessing time, we skip those 3D models with more than 6000 voxels and finally compute the eigenmode of 7,423 3D models. According to the voxel model and eigenmode of each model, we construct the input and output data for the network. For each model, we take 8 randomly initialized vectors and calculate the results of the parallel inverse power method for $m = 10$ eigenvalue intervals. Each object will have 8 data points. The range of the entire eigenvalue interval corresponds to a frequency range of 1000hz-15000hz. The eigenvalue intervals is the same across all objects in dataset. We divide the dataset into a training set, a test set, and a validation set at a ratio of 4:1:1.

We generate an acoustic transfer dataset based on the eigenmode dataset. For each model in the eigenmode dataset, we take the iteration results of the first random initial vector (a total of 8 iteration results, corresponding to 8 initialized vectors). For each iteration result, we set the 10 vectors (corresponding to 10 intervals) as the vibration shape of the object and compute 10 FFAT maps respectively where the frequency matches the midpoint of the interval. To balance the sound quality and the difficulty of network learning, we take the resolution of the FFAT map as 64×32 . To solve the acoustic transfer function, we use the library BEMPP [2] on GPU. Due to limited video memory, we ignore complex models and finally compute acoustic transfer data of 5,239 models. We divide the dataset into a training set, a test set, and a validation set at a ratio of 4:1:1.

8.2. Network Training

When training the network for eigenmode computations, we take the weight parameters in the loss function as $\lambda_F = 5$, $\lambda_r = 200$, $\lambda_p = 0.2$ and standardize the input and output to unit variance. When training the network for acoustic transfer, we also normalize the input and output to unit

variance. Possible data augmentation (mirror and rotation) is used during training. Both networks are optimized by an Adam optimizer, with learning rates of $5e-4$ and $2e-3$ and decays to 0.8 times after every 10 epochs and every 50 epochs, respectively. We finally store the network parameters with the smallest loss in the validation set.

9. Experiments and Results

Our learning-based solver can provide a complete end-to-end 3D modal sound model including eigenmode computation and acoustic transfer data. This computation can be performed in real-time. We evaluate the results and demonstrate the benefits of our method’s prediction accuracy, sound fidelity, and efficiency through comparisons with the ground truth data computed using a physically-based sound synthesis algorithm.

9.1. Implementation

The generalized eigenvalue decomposition function we use is a function in Python Library Scipy (`scipy.sparse.linalg.eigsh`). The function is a wrapper to the ARPACK SSEUPD and DSEUPD functions, which use the Implicitly Restarted Lanczos Method to find the eigenvalues and eigenvectors and similar solvers are used in [46, 19, 5]. This function can be computed in parallel on a CPU. Recent work reported that only a $6.4\times$ speedup can be obtained using two high-end GPUs (NVIDIA Tesla P100s) [9], which shows that GPU acceleration is not significant for generalized eigendecomposition of large sparse matrices. The BEM solver we use is Bempp, a Boundary element method Python package, which supports GPU parallelization. We implement our algorithm on a PC with Intel i7-8700 CPU, and GeForce GTX 1080 Ti GPU. Our neural network is implemented with Minkowski Engine[7] and Pytorch[32] based on Cuda 11.1.

9.2. Prediction for Eigenmode Computation

To analyze the accuracy of our learning-based solver for eigenmode computation, we randomly select several models from the test set and compute approximation eigenmode matrices (defined in ??) using an accurate generalized eigenvalue decomposition solver (ground truth) as well as our learning-based solver. We compare the running time of both these solves and measure the error between the results of our solver and the ground-truth. The error we measure includes the error of the mode shape (eigenvector) and the error of the mode frequency (*Rayleigh quotient*). Our formulation of mode shape accuracy is similar to the definition of peak signal-to-noise ratio (PSNR):

$$10 \cdot \log_{10} \left(\frac{MAX_I^2}{MSE} \right), \quad (13)$$

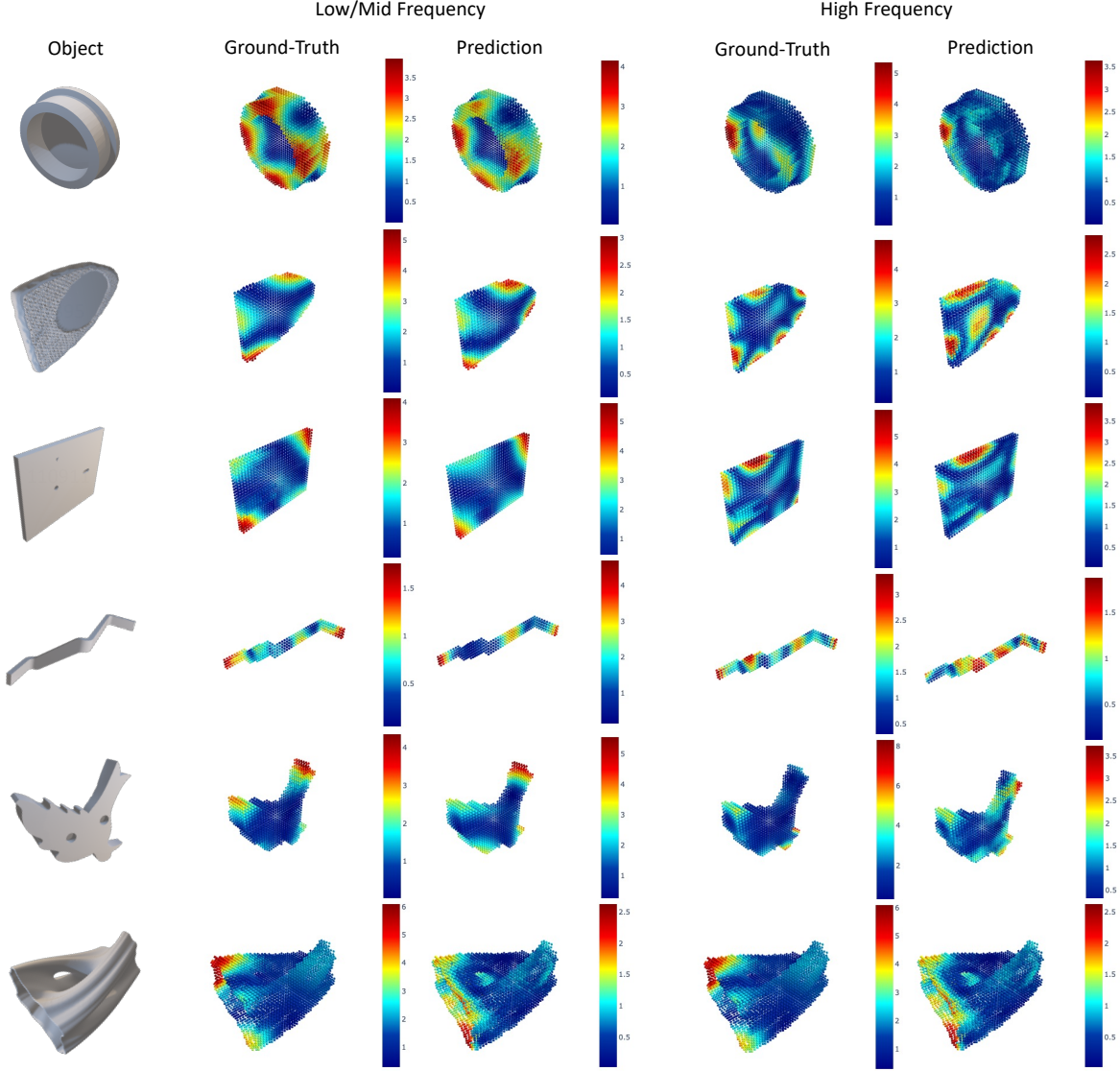


Figure 5. Eigenvectors of low/mid-frequency and high frequency computed by our learning-based solver and traditional eigendecomposition solver (i.e., the ground truth), respectively. The colored scale indicates the length of the displacement vector of each voxel. Our method can generate results similar to the ground-truth (especially in low and mid frequencies) but runs $10\times$ - $100\times$ faster as compared to the traditional solver. Numerical results are shown in Table 1.

where MAX_I and MSE are the max value and mean square error for all eigenvectors. The definition of frequency error is:

$$\text{avg}_i \left| \frac{r_i - \hat{r}_i}{\Delta r_i} \right|, \quad (14)$$

where $r_i - \hat{r}_i$ refers to the frequency difference between prediction and the ground-truth on the mel scale. Δr_i is the length of each interval in the mel scale. All the comparison results are shown in Table 1. The error between our prediction and the ground-truth method is small, but our solver runs significantly faster. The visual comparison eigenmode data is shown in Figure 5. Our predicted eigenvectors exhibit very structure with those computed by a classic solver

(Lanczos algorithm).

9.3. Prediction of Acoustic Transfer Data

We perform a similar evaluation of our learning-based solver for acoustic transfer data. We select several models from the test set and calculate the FFAT map using an accurate BEM solver and our learning-based solver. While calculating the FFAT map, two methods use similar approximation, i.e., the eigenvalues of all modes in an eigenvalue interval are considered as the midpoints of the intervals. Based on this approximation, we compare the speed of the two methods and compute the error in the FFAT map predicted by our learning-based solver. The formulation of the

Table 1. Performance statistics of our learning-based solver for approximate eigenmode (defined in ??) prediction. All timings are given in terms of the total wall clock time. Our solver solves 5 random initial vectors in parallel, and this timing also includes PCA computation for resulting eigenvectors. The mode shape error and frequency error are provided along with the overall speedup. Note that the uncompressed eigenmode dataset of the full test set has size 5.7GB. Our DeepEigen method can predict the eigenmode at runtime and only requires 50MB for network parameters storage. *Mean* indicates the statistics obtained from all testing objects in the dataset.

Object		Accuracy / Error		Comparison		
ID	Voxel	Shape Acc	Freq Err	Lanczos	Ours	Speedup
1	4976	21.08dB	0.40	5.60s	53ms	105×
2	2089	18.07dB	0.17	0.86s	30ms	28×
3	2664	20.84dB	0.22	1.29s	36ms	34×
4	526	14.60dB	0.40	0.07s	22ms	3×
5	3129	20.37dB	0.14	1.36s	38ms	34×
6	5684	18.35dB	0.33	10.27s	53ms	191×
7	9009	31.9dB	0.20	35.64s	92ms	385×
8	11018	21.3dB	0.08	29.40s	106ms	274×
Mean	4619	22.62dB	0.31	22.87s	52ms	440×

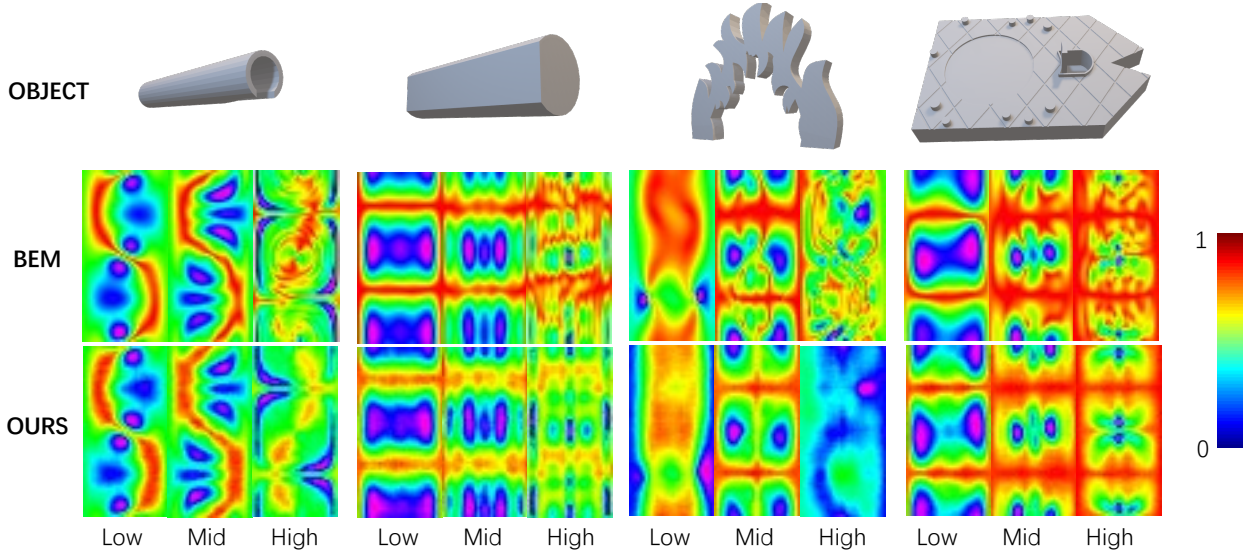


Figure 6. We visualize the results of our network’s prediction using the FFAT map for low, mid, and high frequencies. We compare the results of a BEM solver (top row) and our learning method (bottom row). The colored scale indicates the value in the FFAT maps. Our method can produce results similar to the BEM solver (especially at low and mid frequencies) while obtaining 1000×-10000× speedup.

error is based on KleinPAT [43], which is the spatial average of the difference between two sound pressure amplitudes in decibels (dB):

$$\text{avg}_{\theta, \phi} \left| 20 \log_{10} \left(\frac{\psi(\theta, \phi)}{\hat{\psi}(\theta, \phi)} \right) \right|. \quad (15)$$

The final recorded error is averaged over all the intervals. All the comparison results are shown in Table 2. As compared to KleinPAT[43], our solver’s speed is much faster while maintaining high accuracy. We also visually illustrate that results in Figure 6.

9.4. End-to-End Modal Sound Synthesis

Overall, our learning-based approach achieves real-time performance in terms of modal synthesis and acoustic transfer function computation. Eigenmode data compression and reuse are no longer issues in our approach since complete data prediction can be achieved for any solid object at runtime. Thus, it is no longer necessary to store pre-computed data before runtime sound rendering. Instead, we only store the weights of a deep neural network, which has a lower storage overhead as compared to the eigenmode data. To illustrate that our learning-based solver can provide a complete end-to-end 3D modal sound model, we also evaluate the results on standard benchmarks and provide an example of sound synthesis using our learning-based method for

Table 2. Performance statistics for FFAT maps prediction that are similar to Table 1. The BEM algorithm and our solver both run on a GPU. The FFAT map errors are provided along with the overall speedup. *Mean* indicates the statistics obtained from all testing objects in the dataset.

Object		Error	Comparison		
ID	Surf Voxel		BEM	Ours	Speedup
1	766	2.47dB	1.6mins	11ms	8675×
2	1080	5.71dB	2.5mins	19ms	7999×
3	1312	4.13dB	4.1mins	11ms	22347×
4	1595	3.29dB	4.6mins	10ms	27494×
5	3128	4.04dB	16.9mins	120ms	8457×
6	902	4.18dB	2.5mins	13ms	11357×
7	976	4.64dB	2.1mins	11ms	11536×
8	1820	3.64dB	7.1mins	14ms	30301×
9	1792	4.13dB	9.7mins	13ms	44610×
Mean	1513	4.03dB	6.4mins	14ms	27429×

deformed objects (as shown in the video).

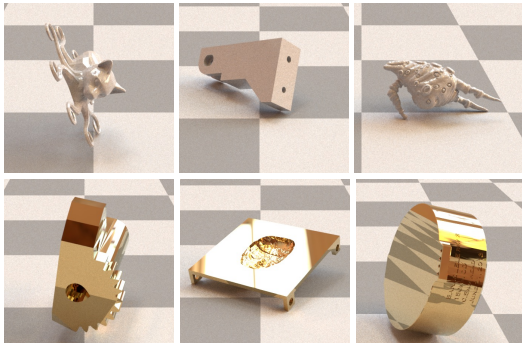


Figure 7. Screenshots of our drop test videos used in the user study. We selected three ceramic models (upper row) and three steel models (bottom row) for the drop test. For each model, we use our learning-based method and physics-based method to synthesize sound. Please see the accompanying video for the sound results.

9.5. Perceptual Evaluation

We conducted a preliminary user study to evaluate the sound quality generated by DeepEigen. Our goal is to verify that our method generates plausible sounds that are comparable to physically-based methods. In total, 80 participants (each with normal hearing) were enrolled in this test and we ensured that each participant has the proper listening device. We showed them videos of six drop scenes shown in Fig. 7 and supplementary material. Each video is composed of two audio-video fragments, one generates sound using a physically-based sound synthesis algorithm, the other generates sound from our approach, Deep-Eigen. Each participant is asked to listen to these videos with no time limit.

Immediately after each video, participants were asked to give a sound reality rating using a 7-point Likert scale ranging from 1 (no similarity at all) to 7 (no difference at all) to measure their similarity. The participants were asked to rate for each video. Although we believe that the standard

of being plausible or realistic can vary among participants, we only asked them for similarity characteristics. The average completion time for each user is 5 minutes. The results show that the mean score is 5.2, which indicates relatively high similarity and indicates that the resulting sound quality is comparable to a physically-based approach.

10. conclusion, Limitations and Future

We present a novel learning-based approach for the sound synthesis of arbitrary solid objects. Our formulation does not need to precompute any eigenmode data and can be applied to deforming or breaking objects. Our network design is motivated by the iterative steps used for eigendecomposition and their connection with 3D sparse computations in a 3D U-Net. We evaluate the accuracy on many complex benchmarks and highlight the benefits in terms of speedups over prior accurate methods. Overall, this is the first learning approach that can approximate the physically-based 3D modal sound synthesis pipeline along with acoustic transfer function computation.

Our method has some limitations. Our training dataset is not very large and the network hyperparameters have not been fine-tuned. Despite good performance on some objects, our method does not exhibit good accuracy in terms of high-frequency prediction. Moreover, our network assumes that the material properties are fixed, and we need to repeat the training step to get different network weights for different materials. In our current formulation, we ignore the radiation efficiency and other techniques used to improve sound fidelity.

There are many avenues for future work. Besides overcoming the limitations, we need a better predictor for high-frequencies and take into account the damping effects. We would also like to develop similar learning-based approaches for complex model sound synthesis. Finally, we would like to integrate and evaluate our method with interactive applications, including games and VR.

References

- [1] W. E. Arnoldi. The principle of minimized iterations in the solution of the matrix eigenvalue problem. *Quarterly of applied mathematics*, 9(1):17–29, 1951.
- [2] T. Betcke and M. W. Scroggs. Bempp-cl: A fast python based just-in-time compiling boundary element library. *Journal of Open Source Software*, 6(59):2879, 2021.
- [3] N. Bonneel, G. Drettakis, N. Tsingos, I. Viaud-Delmon, and D. James. Fast modal sounds with scalable frequency-domain synthesis. In *ACM SIGGRAPH 2008 papers*, pages 1–9. 2008.
- [4] W. L. Briggs, V. E. Henson, and S. F. McCormick. *A multigrid tutorial*. SIAM, 2000.
- [5] J. N. Chadwick, S. S. An, and D. L. James. Harmonic shells: a practical nonlinear sound model for near-rigid thin shells. *ACM Transactions on Graphics*, 28(5):1–10, 2009.
- [6] J. N. Chadwick, C. Zheng, and D. L. James. Pre-computed acceleration noise for improved rigid-body sound. *ACM Transactions on Graphics (Proceedings of SIGGRAPH 2012)*, 31(4), Aug. 2012.
- [7] C. Choy, J. Gwak, and S. Savarese. 4d spatio-temporal convnets: Minkowski convolutional neural networks. In *Proceedings of the IEEE Conference on Computer Vision and Pattern Recognition*, pages 3075–3084, 2019.
- [8] P. R. Cook. Integration of physical modeling for synthesis and animation. In *Proceedings of the 1995 International Computer Music Conference, ICMC 1995, Banff, AB, Canada, September 3-7, 1995*. Michigan Publishing, 1995.
- [9] A. Dziekonski and M. Mrozowski. A gpu solver for sparse generalized eigenvalue problems with symmetric complex-valued matrices obtained using higher-order fem. *IEEE Access*, 6:69826–69834, 2018.
- [10] Z. Fan, V. Vineet, H. Gamper, and N. Raghuvanshi. Fast acoustic scattering using convolutional neural networks. In *ICASSP 2020-2020 IEEE International Conference on Acoustics, Speech and Signal Processing (ICASSP)*, pages 171–175. IEEE, 2020.
- [11] F. Gao, Y. Yang, J. Wang, J. Sun, E. Yang, and H. Zhou. A deep convolutional generative adversarial networks (dcgans)-based semi-supervised method for object recognition in synthetic aperture radar (sar) images. *Remote Sensing*, 10(6):846, 2018.
- [12] B. Graham, M. Engelcke, and L. van der Maaten. 3d semantic segmentation with submanifold sparse convolutional networks. *CVPR*, 2018.
- [13] B. Graham and L. van der Maaten. Submanifold sparse convolutional networks. *arXiv preprint arXiv:1706.01307*, 2017.
- [14] S. H. Hawley, V. Chatziannou, and A. Morrison. Synthesis of musical instrument sounds: Physics-based modeling or machine learning. *Phys. Today*, 16:20–28, 2020.
- [15] K. He, X. Zhang, S. Ren, and J. Sun. Deep residual learning for image recognition. In *Proceedings of the IEEE conference on computer vision and pattern recognition*, pages 770–778, 2016.
- [16] D. L. James. Physically based sound for computer animation and virtual environments. In *ACM SIGGRAPH 2016 Courses*, SIGGRAPH ’16, New York, NY, USA, 2016. Association for Computing Machinery.
- [17] D. L. James, J. Barbič, and D. K. Pai. Precomputed acoustic transfer: Output-sensitive, accurate sound generation for geometrically complex vibration sources. *ACM Trans. Graph.*, 25(3):987–995, July 2006.
- [18] S. Ji, J. Luo, and X. Yang. A comprehensive survey on deep music generation: Multi-level representations, algorithms, evaluations, and future directions. *arXiv preprint arXiv:2011.06801*, 2020.
- [19] X. Jin, S. Li, T. Qu, D. Manocha, and G. Wang. Deep-modal: Real-time impact sound synthesis for arbitrary shapes. In *Proceedings of the 28th ACM International Conference on Multimedia, MM ’20*, page 1171–1179, New York, NY, USA, 2020. Association for Computing Machinery.
- [20] A. Kanezaki, Y. Matsushita, and Y. Nishida. Rotationnet: Joint object categorization and pose estimation using multiviews from unsupervised viewpoints. In *Proceedings of the IEEE Conference on Computer Vision and Pattern Recognition*, pages 5010–5019, 2018.
- [21] A. V. Knyazev. Toward the optimal preconditioned eigensolver: Locally optimal block preconditioned conjugate gradient method. *SIAM journal on scientific computing*, 23(2):517–541, 2001.
- [22] C. Lanczos. *An iteration method for the solution of the eigenvalue problem of linear differential and integral operators*. United States Governm. Press Office Los Angeles, CA, 1950.
- [23] T. R. Langlois, S. S. An, K. K. Jin, and D. L. James. Eigenmode compression for modal sound models. *ACM Transactions on Graphics (Proceedings of SIGGRAPH 2014)*, 33(4), Aug. 2014.
- [24] R. B. Lehoucq, D. C. Sorensen, and C. Yang. *ARPACK users’ guide: solution of large-scale eigenvalue prob-*

lems with implicitly restarted Arnoldi methods. SIAM, 1998.

- [25] D. Li, Y. Fei, and C. Zheng. Interactive acoustic transfer approximation for modal sound. *ACM Trans. Graph.*, 35(1), 2015.
- [26] S. Liu and D. Manocha. Sound synthesis, propagation, and rendering: A survey. *arXiv preprint arXiv:2011.05538*, 2020.
- [27] J. Long, E. Shelhamer, and T. Darrell. Fully convolutional networks for semantic segmentation. In *Proceedings of the IEEE conference on computer vision and pattern recognition*, pages 3431–3440, 2015.
- [28] D. Maturana and S. Scherer. Voxnet: A 3d convolutional neural network for real-time object recognition. In *2015 IEEE/RSJ International Conference on Intelligent Robots and Systems (IROS)*, pages 922–928. IEEE, 2015.
- [29] R. Mehra, N. Raghuvanshi, L. Antani, A. Chandak, S. Curtis, and D. Manocha. Wave-based sound propagation in large open scenes using an equivalent source formulation. *ACM Transactions on Graphics (TOG)*, 32(2):1–13, 2013.
- [30] A. Newell, K. Yang, and J. Deng. Stacked hour-glass networks for human pose estimation. In *European conference on computer vision*, pages 483–499. Springer, 2016.
- [31] J. F. O’Brien, C. Shen, and C. M. Gatchalian. Synthesizing sounds from rigid-body simulations. In *Proceedings of the 2002 ACM SIGGRAPH/Eurographics Symposium on Computer Animation*, SCA ’02, page 175–181, New York, NY, USA, 2002. Association for Computing Machinery.
- [32] A. Paszke, S. Gross, S. Chintala, G. Chanan, E. Yang, Z. DeVito, Z. Lin, A. Desmaison, L. Antiga, and A. Lerer. Automatic differentiation in pytorch. In *NIPS-W*, 2017.
- [33] C. R. Qi, H. Su, K. Mo, and L. J. Guibas. Pointnet: Deep learning on point sets for 3d classification and segmentation. In *Proceedings of the IEEE conference on computer vision and pattern recognition*, pages 652–660, 2017.
- [34] C. R. Qi, L. Yi, H. Su, and L. J. Guibas. Pointnet++: Deep hierarchical feature learning on point sets in a metric space. In *Advances in neural information processing systems*, pages 5099–5108, 2017.
- [35] N. Raghuvanshi and M. C. Lin. Interactive sound synthesis for large scale environments. In *Proceedings of the 2006 symposium on Interactive 3D graphics and games*, pages 101–108, 2006.
- [36] O. Ronneberger, P. Fischer, and T. Brox. U-net: Convolutional networks for biomedical image segmentation. In *International Conference on Medical image computing and computer-assisted intervention*, pages 234–241. Springer, 2015.
- [37] A. Rungta, C. Schissler, R. Mehra, C. Malloy, M. Lin, and D. Manocha. Syncopation: Interactive synthesis-coupled sound propagation. *IEEE transactions on visualization and computer graphics*, 22(4):1346–1355, 2016.
- [38] A. Sterling and M. C. Lin. Interactive modal sound synthesis using generalized proportional damping. In *Proceedings of the 20th ACM SIGGRAPH Symposium on Interactive 3D Graphics and Games*, pages 79–86, 2016.
- [39] A. Sterling, N. Rewkowski, R. L. Klatzky, and M. C. Lin. Audio-material reconstruction for virtualized reality using a probabilistic damping model. *IEEE transactions on visualization and computer graphics*, 25(5):1855–1864, 2019.
- [40] H. Su, S. Maji, E. Kalogerakis, and E. Learned-Miller. Multi-view convolutional neural networks for 3d shape recognition. In *Proceedings of the IEEE international conference on computer vision*, pages 945–953, 2015.
- [41] Z. Tang, H.-Y. Meng, and D. Manocha. Learning acoustic scattering fields for dynamic interactive sound propagation. In *2021 IEEE Virtual Reality and 3D User Interfaces (VR)*, pages 835–844. IEEE, 2021.
- [42] K. van den Doel, P. G. Kry, and D. K. Pai. Foleyautomatic: Physically-based sound effects for interactive simulation and animation. *SIGGRAPH ’01*, New York, NY, USA, 2001. Association for Computing Machinery.
- [43] J.-H. Wang and D. L. James. Kleinpat: Optimal mode conflation for time-domain precomputation of acoustic transfer. *ACM Trans. Graph.*, 38(4):122:1–122:12, July 2019.
- [44] Z. Wu, S. Song, A. Khosla, F. Yu, L. Zhang, X. Tang, and J. Xiao. 3d shapenets: A deep representation for volumetric shapes. In *Proceedings of the IEEE conference on computer vision and pattern recognition*, pages 1912–1920, 2015.
- [45] Q. Zhang, L. Ye, and Z. Pan. Physically-based sound synthesis on gpus. In *International Conference on Entertainment Computing*, pages 328–333. Springer, 2005.
- [46] C. Zheng and D. L. James. Rigid-body fracture sound with precomputed soundbanks. In *ACM SIGGRAPH 2010 Papers, SIGGRAPH ’10*, New York, NY, USA, 2010. Association for Computing Machinery.

- [47] C. Zheng and D. L. James. Toward high-quality modal contact sound. In *ACM SIGGRAPH 2011 papers*, pages 1–12. 2011.
- [48] Q. Zhou and A. Jacobson. Thingi10k: A dataset of 10,000 3d-printing models. *arXiv preprint arXiv:1605.04797*, 2016.